

**Interferometry at Mid-Infrared Wavelengths: The ISI System**  
**C.H. Townes and E.H. Wishnow**  
**University of California at Berkeley**

The ISI (Infrared Spatial Interferometer) involves three movable telescopes of Pfund design, each in trailers, each with a radiation collecting mirror 65 inches in diameter. The telescopes can be moved, and then set down on concrete pads for stability. They are located on Mt. Wilson, where pads have been arranged to give baselines varying from 4 to approximately 75 meters and oriented in various directions. Initial work, between 1988 and 2002, was done with two telescopes; the third telescope was added in 2003.

**Description and Functioning of the Interferometer System.**

The telescopes involve heterodyne detection of stellar signals at wavelengths near  $11 \mu\text{m}$ , with laser local oscillators which in the detectors beat with stellar signals. Beat frequencies are generated and amplified over a frequency range of approximately  $3 \times 10^9$  Hz giving a detected bandwidth of twice that because of the superposition of upper and lower sidebands. This bandwidth is limited by the response time of the solid state detectors. Each telescope has its own  $\text{CO}_2$  laser local oscillator, but laser signals are sent between the three telescopes, allowing the three lasers to be locked in phase with small frequency differences chosen to be in the range 50 – 200 Hz. Stellar signals from each pair of telescopes are combined, producing interference signals centered on the frequency differences of the two lasers in the two telescopes.

A picture of two telescopes separated by 4 meters, the minimum baseline, is shown in Figure 1. Figure 2 gives a schematic of a single telescope. Figures 3 and 4 show schematics of the signal arrangement for producing interference fringes.

There are advantages and disadvantages to heterodyne detection at infrared wavelengths. The primary disadvantage is lower sensitivity than most direct detections. Heterodyne detection has a fundamental minimum noise corresponding to a noise

temperature of  $\frac{h\nu}{k}$ . In the microwave region this is not a dominant source of noise. But at the ISI wavelengths near  $11 \mu m$ , this noise temperature is approximately 1300 K, and usually dominates other noise sources. For detection of continuum radiation, the ratio of

noise for the ISI's heterodyne detection to that for direct detection is  $\frac{1300}{T_D} \sqrt{\frac{\Delta\nu_D}{6 \times 10^9}}$ ,

where  $T_D$  is the noise temperature of direct detection, perhaps near 300 K, and  $\Delta\nu_D$  is the direct detection bandwidth, often as large as  $250 \text{ cm}^{-1}$  or  $7.5 \times 10^{12}$  Hz. The ratio of sensitivity would then be approximately 150. However, for spectral lines, where the bandwidth needed would be narrow and comparable to  $6 \times 10^9$  Hz ( $=0.2 \text{ cm}^{-1}$ ) the narrow bandwidth of heterodyne spectroscopy is no longer a disadvantage, and generally an advantage in that narrow lines can be easily measured. In addition, the noise temperature for narrow band direct detection generally goes up as bandwidth becomes very narrow and can easily be as large as that for heterodyne detection, so that sensitivities are comparable.

The ISI's narrow bandwidth means that, for good interference fringes, the separation between telescopes need not be superaccurate. The required accuracy is a

modest fraction, perhaps  $\frac{1}{20}$  of  $\frac{c}{\Delta\nu}$ , which is  $=\frac{1}{4} \text{ cm}$ . Interferometry at wider

bandwidths, generally used for direct detection, requires much more precise delay times

and a constancy in telescope separation of approximately  $\frac{1}{5000} \text{ cm}$  for a bandwidth of

$250 \text{ cm}^{-1}$ .

The mid-IR region is useful for examination particularly of old stars because it can penetrate dust shells around stars much better than can shorter wavelengths. In addition, relatively cool dust around stars radiates mid-IR wavelength but not visible wavelengths, and hence it can also be measured in the mid IR. A difficulty is that there are many IR spectral lines in the gas and dust shells surrounding old stars. Broadband detection does not separate the spectral lines from continua, and hence interpretation of the stellar and shell size is usually quite uncertain. Narrow band measurements, as is provided by heterodyne detection, can easily discriminate between spectral lines and continua by making measurements on or off the spectral lines. Hence narrow band measurements are

desirable and, as noted above, the sensitivity of heterodyne detection for narrow band work is as good or possibly better than that for continuum detection.

Measurements at various wavelengths and bandwidths produce, as a result of dust and atmospheres around stars, a wide variety of apparent sizes of stars. One rather extreme case is WHya, where a measurement at 7 mm wavelength gives a size as large as about 80 mas. However, ISI measurements show that this is due to ionized material around the star, which itself is smaller than about 30 mas. The apparent sizes of stars surrounded by dust have been shown to vary widely with wavelength when measured in the visible and near IR with relatively broad bandwidths. And a variety of apparent sizes of old stars are typically obtained using wide bandwidth measurements in the visible and near IR.

All this makes narrow-bandwidth measurements, especially at mid-IR wavelengths which penetrate the dust rather well, of special value. For an interferometric system with many telescopes, heterodyne detection has another possible advantage. A heterodyne signal is detected in a single telescope, then sent to an amplifier so it can be amplified as much as desired, then divided to be combined with signals from other telescopes to produce interference fringes. Direct detection does not amplify the stellar signal. Hence the stellar light itself from one telescope is usually divided and equal amounts combined with stellar light from other telescopes. For a system of 10 telescopes, individual stellar signals are hence divided into nine equal parts to obtain all the interference signals wanted. This reduces the sensitivity by a factor of 9 (or the number of telescopes minus 1). A different direct detection system, but requiring many pixels for detection, has been developed by Monnier et al<sup>1</sup>. Heterodyne signals do not lose sensitivity by this process of division because of the possibility of amplification before division

The ISI system usually measures stellar and dust continuum and radiation by operating at a frequency where there are no spectral lines. However, it has also been specifically tuned to be on spectral lines so the distribution of particular molecules around stars can be directly measured. For example, NH<sub>3</sub> and SiH<sub>4</sub> have been measured, and found to form in the dust shells some distance from the stars themselves<sup>2</sup>.

The stellar motion across the sky means that for a fixed telescope position the interference signal goes up and down, depending on whether the two signals are in or out of phase. The relative phase of local oscillators in the three ISI telescopes is changed

systematically in such a way that these variations don't occur, so that fringe signals increase and decrease always at a fixed frequency, determined by the relative frequency at which the various laser local oscillators are locked together. Each fringe is hence at a constant frequency except for fluctuations produced by variations in air density along the paths from stars to telescope, which can occur as rapidly as about 10 Hz and are not independently measurable to allow corrections for such pathlength fluctuations. However, under very good atmospheric conditions fringes fluctuate as a result of atmospheric variations at less than  $\frac{1}{100}$  Hz. Figures 5 and 6 show interference fringe signals under rather extreme atmospheric conditions, one exceptional good and providing a very narrow fringe bandwidth, the other quite poor and having a very wide bandwidth.

### Results of Measurements

The ISI has been used primarily to examine size, shapes, and variations in size and shapes of old stars as well as their emission of gas and dust, including the dust distribution, dynamics, and variation with time. The following discussion will initially consider the dust shells around such stars. This will be followed by discussion of findings about the stars themselves.

Visibility of the star  $\alpha$  Ori as a function of resolution or spatial frequency is shown in Figure 7, for which the dust surrounding  $\alpha$  Ori is largely resolved and the star shown to produce about 50% of the 11 micron radiation. Other measures were made at a different time for low resolutions ranging from sfu of 0.2 to 1 (in units of  $10^5$  cycles per radian on the sky). This data fits the low sfu part of the curve shown in Figure 7. The curve fitting measured visibilities in Figure 7 is the result of a model with a thin spherical dust shell surrounding the star at a distance of approximately 1 arc sec from the star.

Some stars may vary periodically in power emitted, giving variations in visibility, as shown in Figure 8 where the visibility curve, due primarily to warm dust surrounding the star, is seen to vary substantially from maximum to minimum luminosity of the star IRC +10216. The curves are fitted by dust models at two different temperatures involving

a spherical distribution of density decreasing as  $\frac{1}{r^2}$  where r is the distance from the star.

However, more detailed measurements at many baselines and with phase closure shows that dust surrounding this star is quite complex, as illustrated in Figure 9. In this case, 11 micron radiation from the star itself is only about 2% of the total. As can be seen from Figure 9, radiation from the dust also varies with time.

Commonly, dust surrounding old stars is approximately spherically distributed. An example is CIT6, for which the visibility curve is shown in Figure 10. It corresponds

to dust expanding uniformly and hence distributed approximately as  $\frac{1}{r^2}$ , where  $r$  is the distance from the star. The phase closure is rather close to zero, measurements giving an actual phase closure of  $6.6^\circ \pm 1.3^\circ$ , so the dust shell is not very asymmetric, in contrast to IRC +10216.

Dust surrounding O Ceti has been observed over some period of time. Measurements with the three telescopes, including phase closure, have been used, for example, to examine the irregularities and changes with time from August 2003 to late 2005. The results are plotted in Figure 11, which shows much structure, asymmetry, and variations in the dust distribution.

Gas and dust may be emitted by the star in a discrete or periodic fashion. This is illustrated in Figure 12, indicating three dust shells surrounding the star NML Tau. The expansion indicated in this figure implies an outward velocity for the two outer shells of about 20 km/sec, which corresponds rather well to doppler velocity measurements of CO spectra and OH maser emission<sup>8</sup>.

There is at least one example where dust surrounding a star has moved surprisingly fast. This is  $\alpha$  Her, for which ISI measurements indicate an expansion velocity of the dust of approximately 75 km/sec<sup>9</sup>.

Overall, ISI measurements show that dust from gas emitted by old stars is quite variable and dynamic, though uniform expansion and a spherical distribution is not a bad approximation for perhaps about 30% of the stars.

Stars themselves can also be quite dynamic, and often not simple uniformly intense spheres. Change in size and brightness have long been recognized to be characteristic of miras. Perhaps the most clear-cut measurement of such a size change was of O Ceti measured by the ISI, and discussed in the next paragraph. For measurement

of stellar size, baselines in the range 12 to 50 meters are generally used by the ISI. The visibility curve ( $vis^2$ ) of  $\alpha$  Ori is shown in Figure 13 for baselines in this range. It gives a diameter for  $\alpha$  Ori of  $54.7 \pm 0.3$  mas at 11 microns<sup>10</sup>, about 14% larger than the first measurement made by Michelson and Pease<sup>11</sup>. This difference is approximately what is to be expected due to “limb darkening”, as predicted by Michelson and Pease<sup>11</sup>. Measurement at mid-IR wavelengths tends to minimize the effects of limb darkening compared to what is found at visible wavelengths, and hence makes the longer wavelengths best for determination of actual stellar sizes.

The first measurement of the change in size of O Ceti (Mira) is shown in Figure 14. Its maximum size is found to occur at a phase of approximately 0.15, or about  $\frac{1}{6}$  of a cycle after the maximum optical luminosity<sup>12</sup>. If a sine curve is fitted to the measurements, it indicates a total change in size of O Ceti of approximately 25% as it goes from maximum to minimum. The amount of change and the phase for maximum size are close to what has been expected theoretically. Several other stars have also been found to change size appreciably. However, their changes have not yet been measured over time systematically, as was done for O Ceti. Hence to what extent their changes are periodic or episodic is not yet determined by the measurements.

With the three telescopes oriented in a triangle, and with phase closure measures, variations of stars from circularity and their asymmetries can be measured, as has been done with the ISI. For example,  $\alpha$  Ori appears to be elliptical with differences between major and minor axes of about 15%, as shown in figure 15. It also was found to be asymmetric, possibly due to a large bright spot. It's unclear how much of the apparent ellipticity may be due primarily to such a bright spot. The measurements can be modeled reasonably well by a spherical star and a bright spot near its edge with about 10% of the entire star's 11 micron luminosity. Such large spots are not unexpected for large old stars such as  $\alpha$  Ori, and probably this is the best explanation of the observations. Clearly further measurements and observation of possible changes over time are very desirable. A few stars other than  $\alpha$  Ori have also been found to be nonspherical, including O Ceti and R Leonis<sup>13</sup>. Precise measurements will presumably show such phenomena in almost all stars, particularly the large and older or very young ones.

## Future Plans

Study of the formation and dynamics of dust shells around stars, and of the formation of molecules around them are clearly highly desirable. Such dynamics are complex, and reasonably complete theoretical interpretation maybe difficult. Non-sphericity and asymmetries in apparent stellar shapes are also fascinating, and perhaps will be more clearly interpretable than the dust dynamics. In any case, it is hoped the ISI can yield many results in both areas. However, for the immediate future it is planned to concentrate on the stars themselves.

Although there are an enormous number of stars for which good interferometric measures would be desirable, it appears most fruitful to concentrate at present on large well-known stars, and their changes with time. With the detailed information now possible by interferometry, it seems best to get as much information on size, shape, asymmetry, spots, and changes with time on well-known stars for which much else is already known, and try to understand the behavior of each in detail. Parallel measurements by other instruments would of course be very desirable, and enhance the clarity and completeness of our understanding.



**Figure 1:** U.C. Berkeley Infrared Spatial Interferometer is shown on its initial 4 m baseline at Mt. Wilson in Southern California. Visible are the two telescopes, each of 65” aperture, which are mounted in modified semi-trailers. Each telescope consists of a flat mirror that tracks the source and a parabolic mirror that is fixed, the latter barely visible on the left of the trailer in the foreground. The parabolic mirror focuses the light through a hole in the flat mirror.

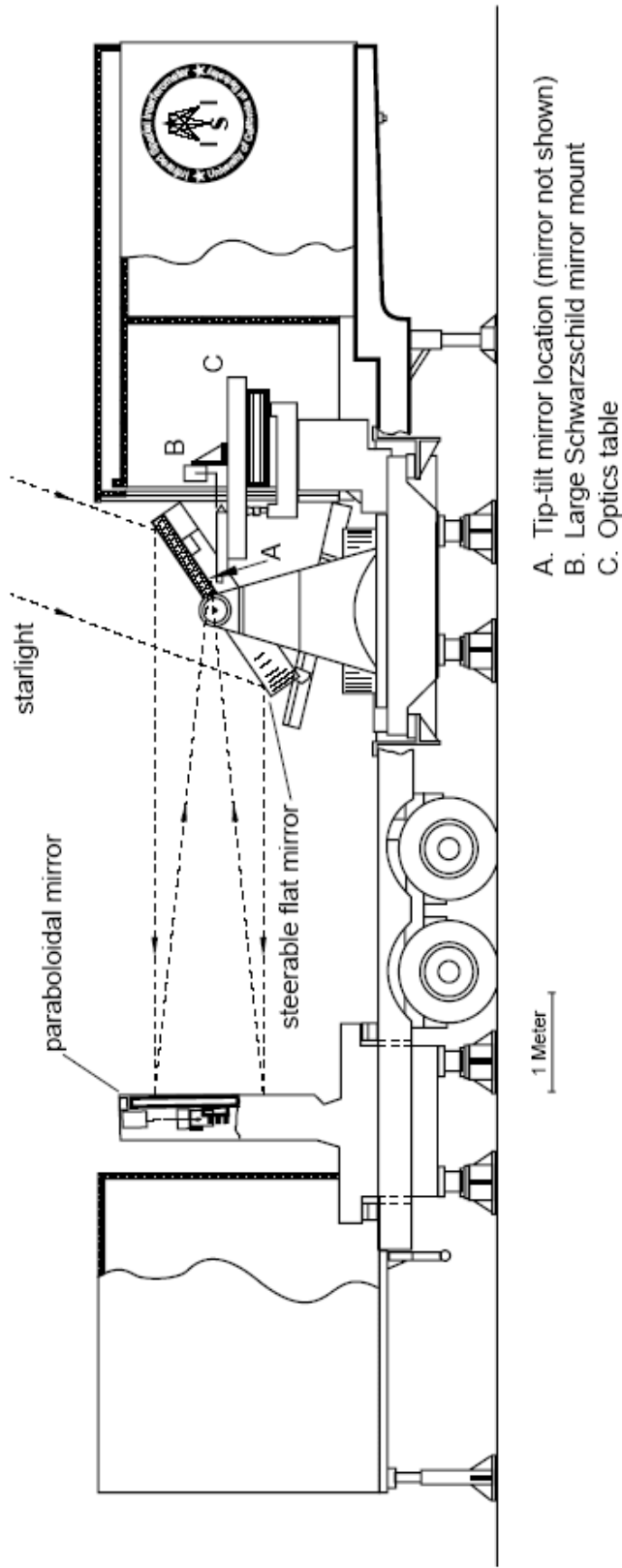


**Figure 2:** Schematic outline of the trailers. The flat mirror mount is to the right, while the mount for the parabolic mirror is to the left.

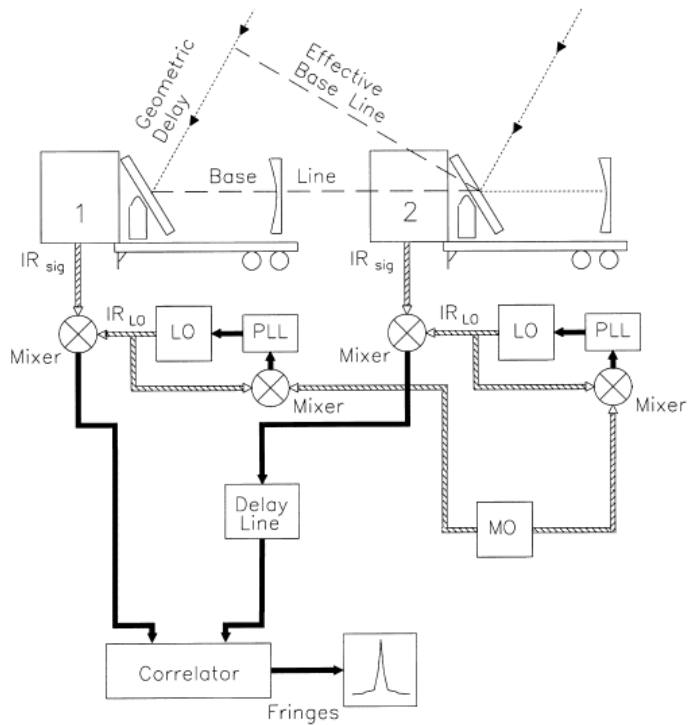


**Figure 3:** A schematic of the ISI Interferometer, showing the local oscillators (LO) and the semiconductor detector-mixers which provide heterodyne detection. The two LOs are locked together in phase by the phase lock loop (PLL) which responds to their beat signal in another detector-mixer. The IF signals from the two telescopes, of bandwidth 3 GHz, are beat together to form a “fringe”.

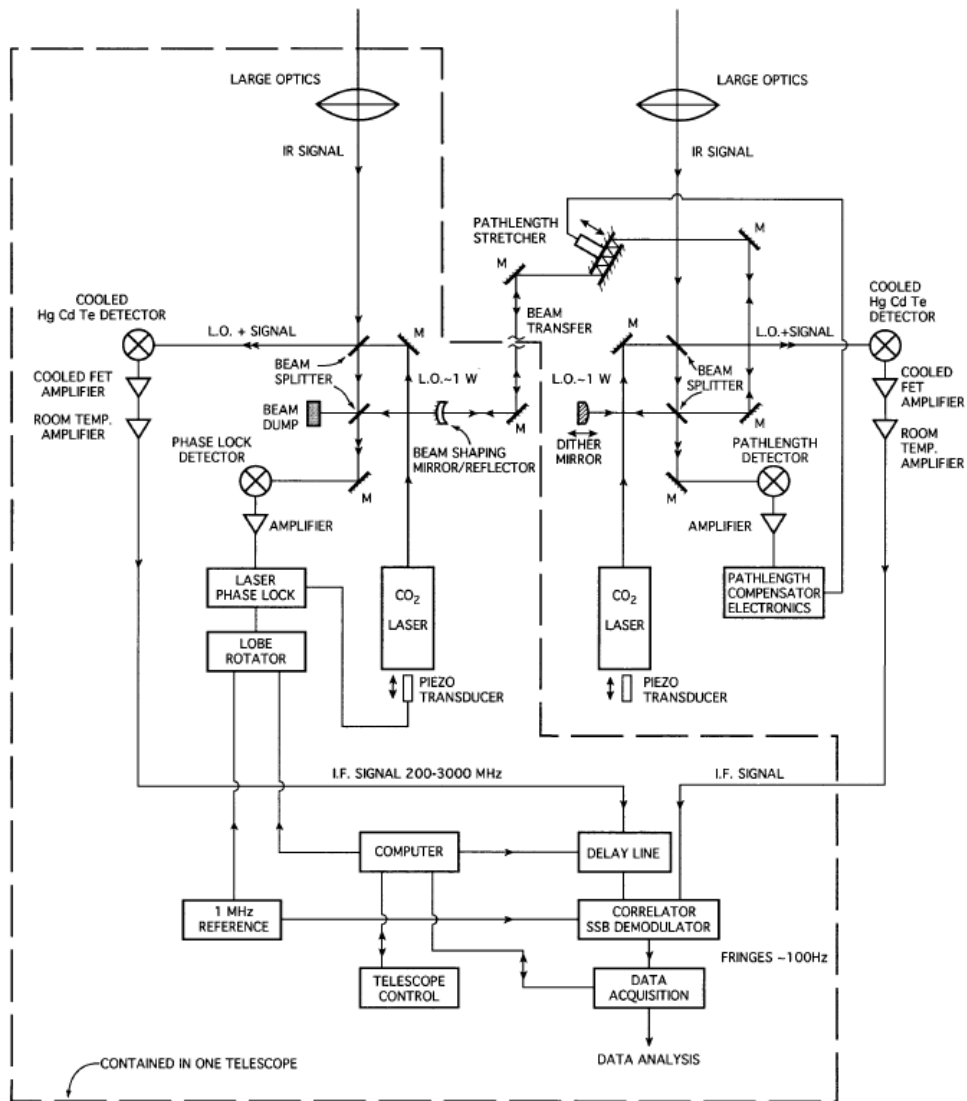


**Figure 4:** Conceptual block diagram of the heterodyne detection system of the interferometer. Shown are the main optical systems as well as some of the signal processing hardware.

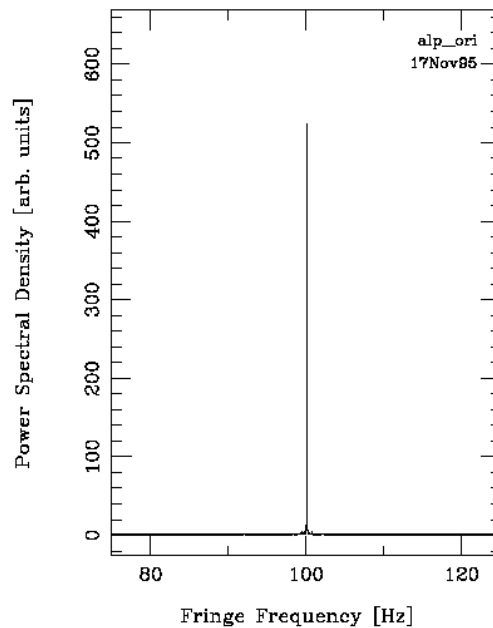
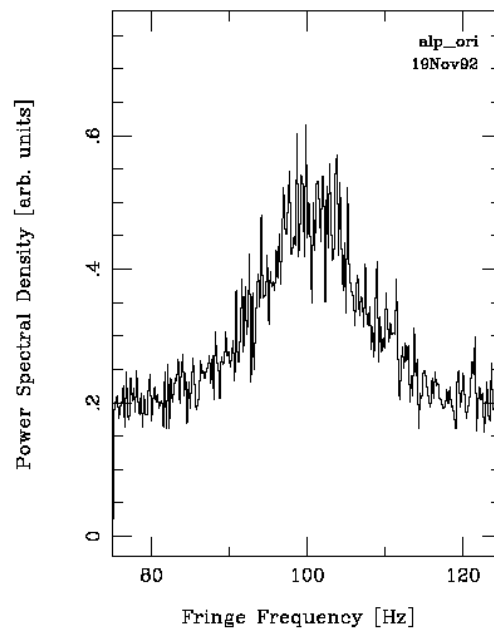


**Figure 5:** An interference fringe signal of  $\alpha$  Orionis under exceptionally good seeing conditions. Atmospheric fluctuations are small enough that only very weak sidebands over a small fraction of one Hertz are produced by their variations. The Data were taken for 512 seconds, and the very narrow resulting fringe has a width due primarily to this finite time of measurement<sup>3</sup>

**Figure 6:** An interference fringe from  $\alpha$  Orionis under very poor seeing conditions. In this case



the atmospheric pathlength is fluctuating severely and on timescales comparable with the inverse width seen, or about 1/15 sec. This is fast for wavelengths as long as 11  $\mu\text{m}$ . In spite of such fluctuations, the fringe magnitude, or total power, can be rather accurately determined by integrating the total power under the curve of this figure<sup>3</sup>.

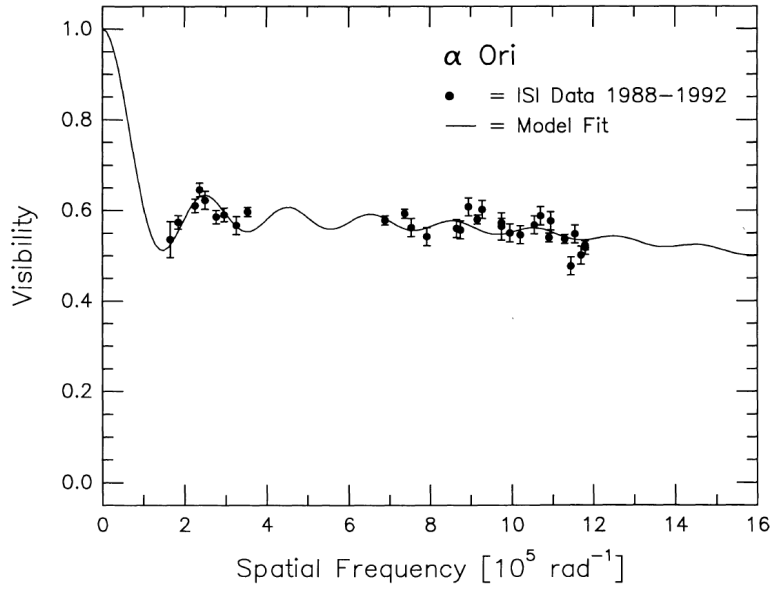


**Figure 7:** The observed visibility curve of  $\alpha$  Orionis as a function of spatial frequency of the interference pattern on the sky. The relative constancy of visibility for spatial frequencies  $>1.0 \times 10^5$  cycles  $\text{rad}^{-1}$  indicates there is very little dust at distances closer than about 1 arc sec. The positions of the first minimum and maximum in the sinusoidal variation which decreases in amplitude towards higher spatial resolution indicates that the inner surface of the dust shell is at 1.0 arc sec radius from the star<sup>4</sup>.

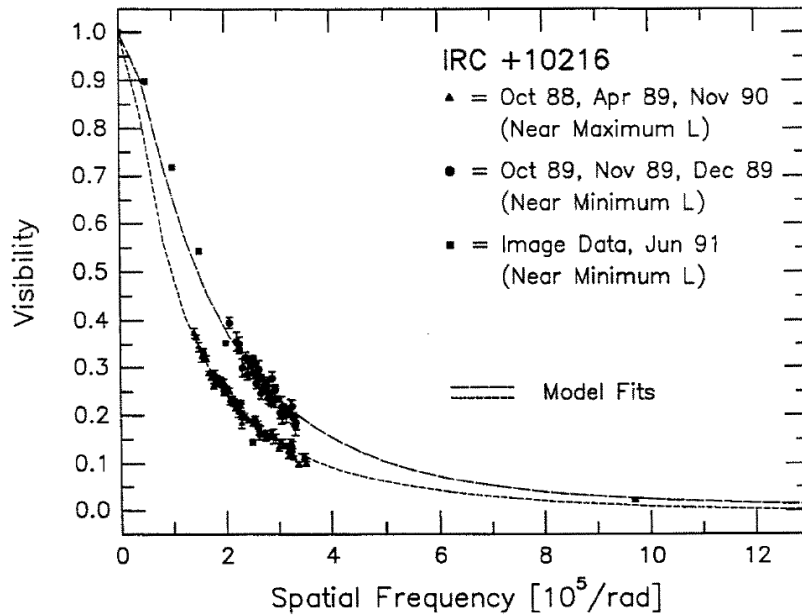


**Figure 8.** Visibility measurements of IRC + 10216 compared for minimum and maximum phase of luminosity (L). The square points represent visibility calculated from an image taken by a multipixel camera.

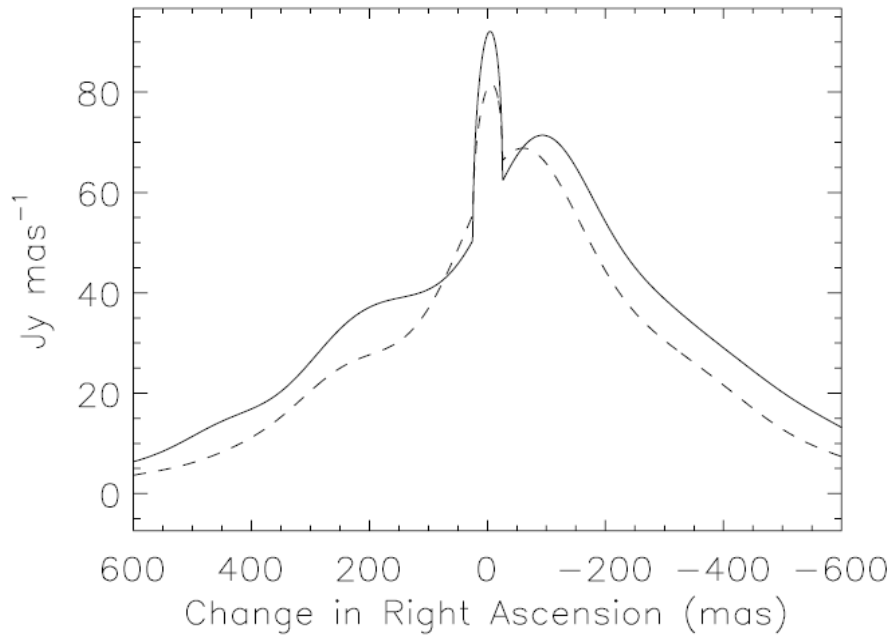


**Figure 9.** One dimensional profile of the  $11\ \mu\text{m}$  intensity of IRC + 10216. The solid line is the image from 2004 data and the dashed is 2006. The relative heights give a ratio of 0.8 for the total flux of the 2006 data to the 2004 data. From  $12\ \mu\text{m}$  IRAS data, the total 2004 flux is taken to be 47,500 Jy. East is to the left<sup>6</sup>.

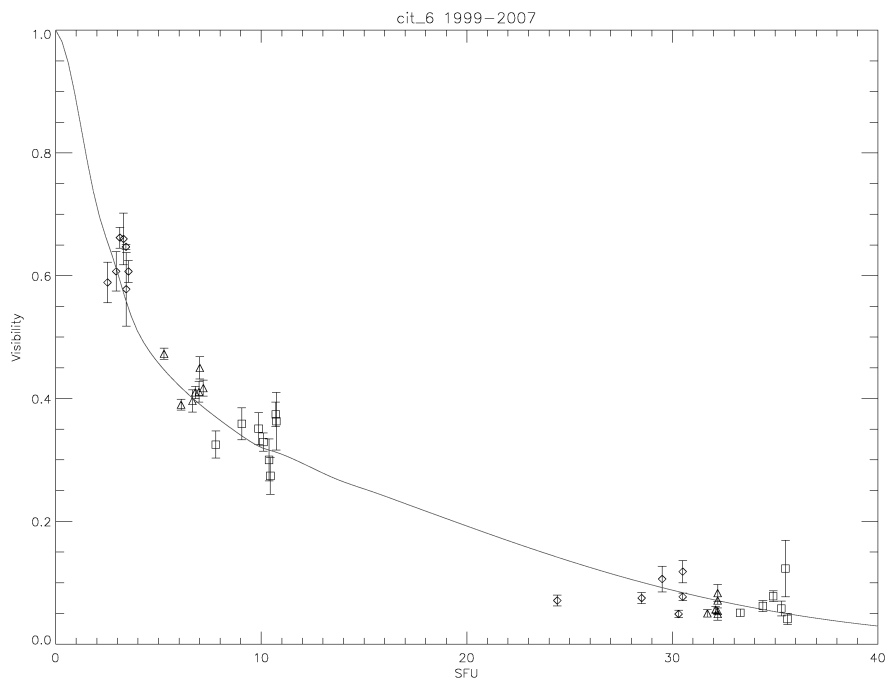


**Figure 10.** Visibility curve for the star CIT6 and its dust shell, measured 1999-2007. sfu represents spatial frequency in units of  $10^5$  per arc sec. The curve fitted to the visibility measurements represents a dust density which varies as  $1/r^2$ , where  $r$  is the distance from the stellar center. The star itself emits very little of the measured  $11 \mu\text{m}$  radiation, as indicated by the very low visibility at  $\text{sfu} \geq 30$ .

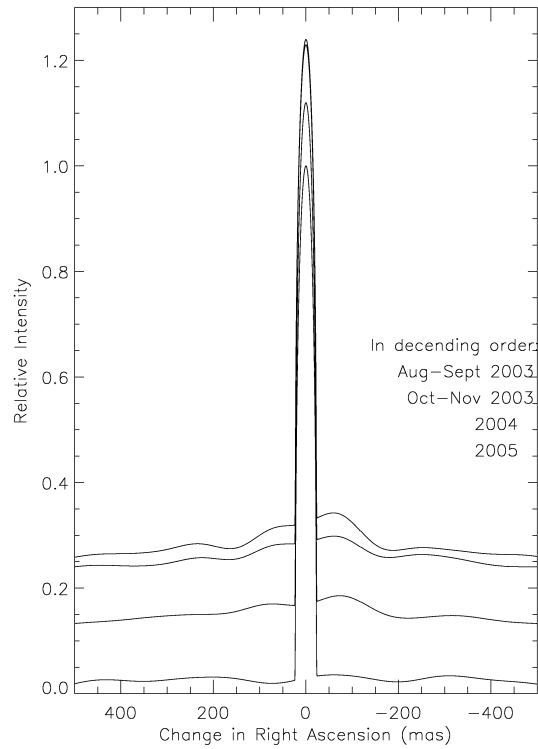


**Figure 11.** One-dimensional profiles of the dust shell surrounding O Ceti over four epochs during Aug. and Sept. of 2003, Oct. and Nov. of 2003 and late 2004 and 2005. The profiles are in descending order with vertical displacement of each image from zero being proportional to time before the last epoch. Each profile is adjusted so that the maximum intensity is equal to unity before displacement. East is left<sup>7</sup>.

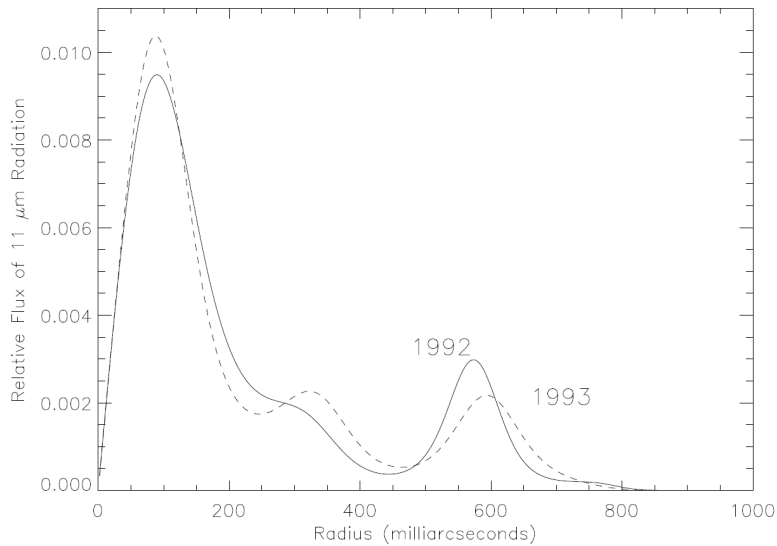


**Figure 12.** Radial intensity distribution of  $11 \mu\text{m}$  radiation dust for NML Tau. Ordinates are proportional to total intensity in a narrow ring about the star of radius given by the abscissae. The solid curve fits the 1992 data, and the dashed one the 1993 data. A more or less periodic shell structure and some motion from 1992 to 1993 is seen<sup>8</sup>

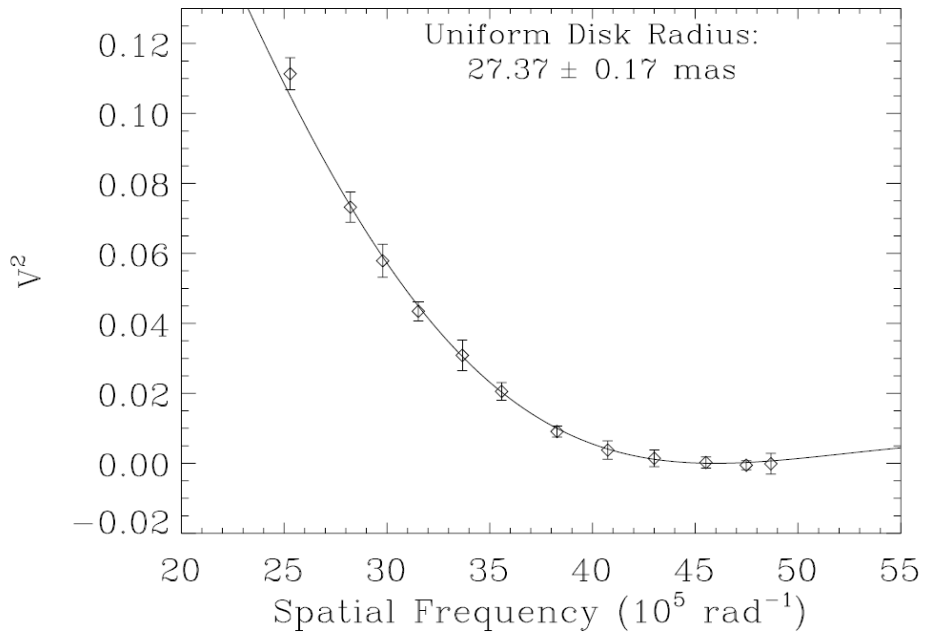


**Figure 13.** Long-baseline visibility squared data from 1999 for Orionis (*individual points*) and uniform disk model fit (*solid curve*). The theoretical curve gives a visibility of zero at a spatial frequency of  $46.0 \times 10^5 \text{ rad}^{-1}$ .<sup>10</sup>

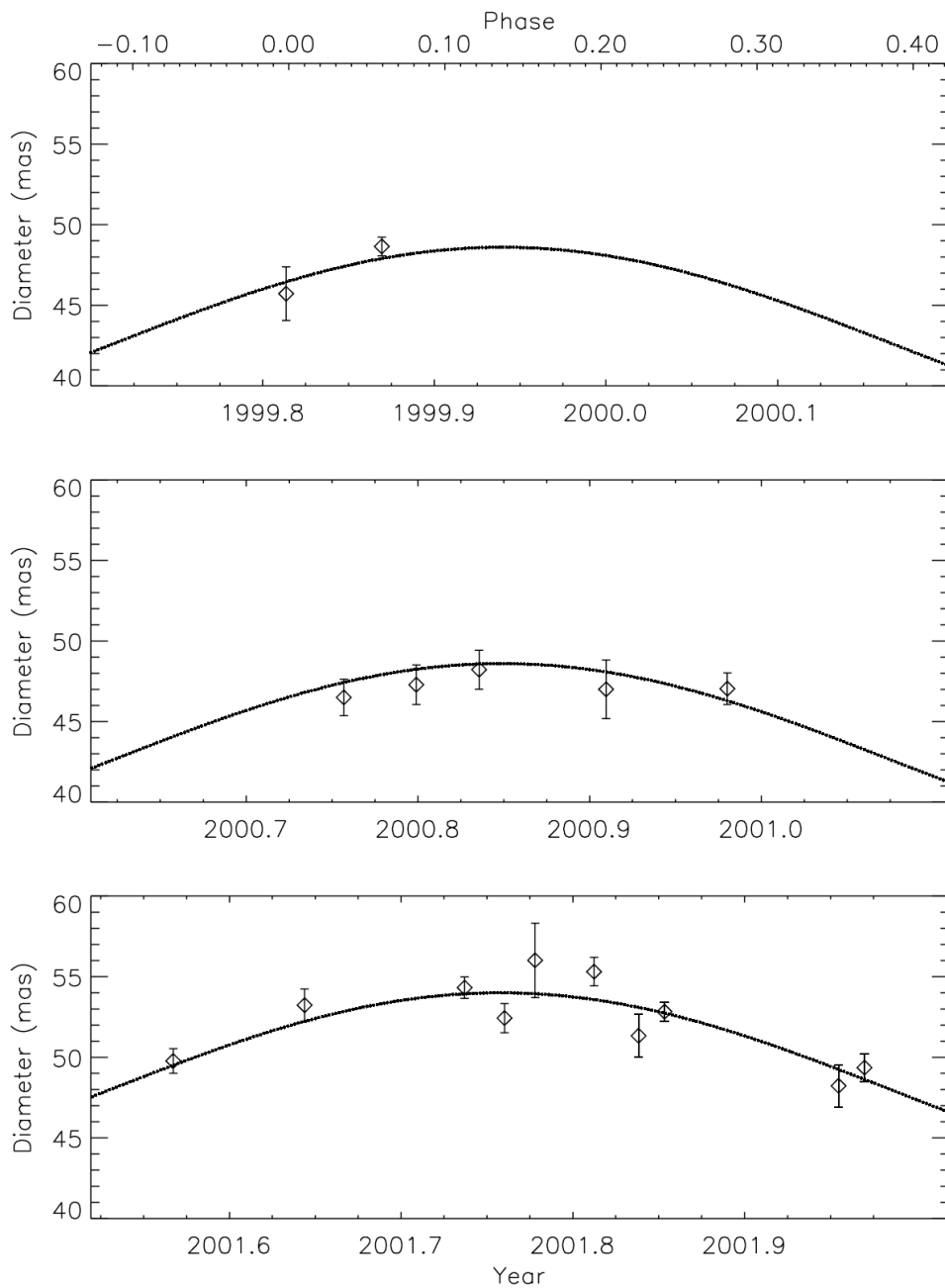


**Figure 14.** Variation of the diameter of O Ceti with phase (given by the top axis) and date. Also plotted is the best-fitting sinusoid having a peak-to-peak amplitude of 12 mas around an average diameter of 48 mas for 2001 and 42.6 mas for 1999 and 2000 and obtaining maximum size at phase 0.135<sup>12</sup>.

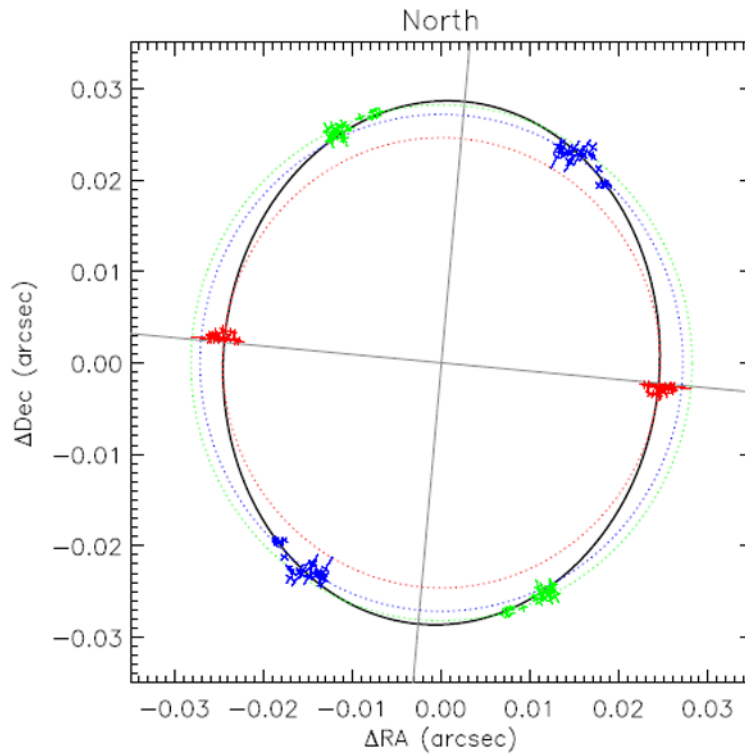


**Figure 15.** Ellipse fit to the visibility data for  $\alpha$  Orionis from three differently oriented baselines. The modeled uniform disk radii for each measurement are plotted on both sides of the star, making each pair of clustered measurements redundant. Circular models fit to the measurements of each baseline individually are shown as dotted circles. North is up and east is left<sup>13</sup>.

1. "Michigan Infrared Combiner (MIRC): Commissioning Results at CHARA Array, J.D. Monnier, E. Pedretti, N. Thureau, J.-P. Berger, R. Milan-Gabet, T. ten Brummelaar, H. McAlister, J. Sturmman, L. Sturmman, A. Tannirkulam, S. Webster, and Z. Ming, SPIE Vol. 6268, pg. 62881 (2006)
2. "Mid-infrared Interferometry on Spectral Lines: III. Ammonia and Silane around IRC +10216 and VY CMa", J. D. Monnier, W. C. Danchi, D. S. Hale, P. G. Tuthill and C. H. Townes. *Ap.J.*, **543**, 868 (2000).
3. "Infrared Spatial Interferometer," C.H. Townes, M. Bester, W.C. Danchi, D.D.S. Hale, J.D. Monnier, E.A. Lipman, P.G. Tuthill, M.A. Johnson, and D. Walters, *Astronomical Interferometry*, Robert D. Reasenberg, (ed.), *SPIE Proceedings* **3350**, 908 (1998).
4. "Heterodyne Interferometry in the Infrared," C.H. Townes, M. Bester, W.C. Danchi, C.G. Degiacomi, and L.J. Greenhill, *Very High Angular Resolution Imaging*, J.G. Robertson and W.J. Tango (eds.) **19**, Kluwer (1994).
5. "An IR Spatial Interferometer at 10  $\mu\text{m}$  Wavelength and Measurement of Stellar Dust Shells," C.H. Townes, M. Bester, W.C. Danchi, C.G. Degiacomi, and L.J. Greenhill, *Infrared Phys. Technol.* **35**, No. 2/3, 503 (1994).
6. "The Radiative Pattern and Asymmetry of IRC+10216 at 11 Microns with Interferometry and Closure Phase, A.A. Chandler, K. Tatebe, D.D.S. Hale, and C.H. Townes, *ApJ*.657, 1042 (2007)
7. "Interferometry on Stars at Mid-Infrared Wavelengths". K. Tatebe, D.D.S. Hale, and C.H. Townes, SPIE Proceedings, Vol. 6678, 6678 G-1 (2007)
8. "Multiple Dust Shells and Motions Around IK Tauri as Seen by Infrared Interferometry," David D.S. Hale, M. Bester, W.C. Danchi, S. Hoss, E. Lipman, J.D. Monnier, P.G. Tuthill, C.H. Townes, M. Johnson, B. Lopez, and T.R. Geballe, *ApJ* **490**, 407 (1997).
9. "Observation of a Burst of High-Velocity Dust from  $\alpha$  - Herculis", K. Tatebe, D.D.S. Hale, E.H. Wishnow, and C.H. Townes, *ApJ. Letters* 658, L103 (2007)
10. "Precision Measurements of the Diameters of  $\alpha$  Orionis and  $\theta$  Ceti at 11 Microns", J. Weiner, W.C. Danchi, D.D.S. Hale, J. McMahon, C.H. Townes, J.D. Monnier, and P.G. Tuthill. *ApJ* **544**, 1097 (2000)
11. "Measurement of the Diameter of  $\alpha$  Orionis with the Interferometer" A.A. Michelson and F.G. Pease, *ApJ* **53**, 249 (1921)
12. "Interferometry on Mira in the Mid-Infrared, Cyclic Variability of the Continuum Diameter and the Effect of Spectral Lines on Apparent Size", J. Weiner, D. D. S. Hale, C. H. Townes, *ApJ*.588, 1064 (2003)

13. “The Nonspherical Shape of Betelgeuse in the Mid-Infrared”, K Tatebe, A.A Chandler, E.H. Wishnow, D.D.S. Hale, C.H. Townes, *Ap.J.* 670, L21 (2007)
14. “The Evolving Shapes of O Ceti and R Leonis, K. Tatebe, E.H. Wishnow, C.S. Ryan, D.D.S. Hale, and C.H. Townes *ApJ* to be published (2008)